Lattice Disordering and Domain Dissolution Transitions in Polystyrene-*block*-poly(ethylene-*co*-but-1-ene)-*block*-polystyrene Triblock Copolymer Having a Highly Asymmetric Composition

Jin Kon Kim* and Hee Hyun Lee

Department of Chemical Engineering and Polymer Research Institute, Pohang University of Science and Technology, Pohang, Kyungbuk 790-784, Korea

Shinichi Sakurai,* Sakae Aida, Junzo Masamoto, and Shunji Nomura

Department of Polymer Science and Engineering, Kyoto Institute of Technology, Sakyo-ku, Kyoto 606-8585, Japan

Yuichi Kitagawa and Yoshikazu Suda

Tuftec Development and Technology Department, Asahi Chemical Industry Co. Ltd., 1-3-1 Yako, Kawasaki-ku, Kawasaki 210-0863, Japan

Received February 25, 1999; Revised Manuscript Received July 20, 1999

ABSTRACT: The lattice disordering transition (LDT) and the domain dissolution transition (DDT) of a highly asymmetric polystyrene-*block*-poly(ethylene-*co*-but-1-ene)-*block*-polystyrene (SEBS-8) triblock copolymer with a volume fraction of polystyrene (PS) block of 0.084 have been investigated by small-angle X-ray scattering (SAXS), transmission electron microscopy (TEM), and rheology. The PS spheres formed in the SEBS-8 sample exhibited a body-centered cubic (bcc) lattice at lower temperatures and underwent disordering in the bcc lattice (so-called LDT) at ∼150 °C. Above this temperature (T_{LDT}), spheres in liquidlike short-range order (LSO) with relatively thin interface between the PS domain and the poly(ethylene-*co*-but-1-ene) (PEB) matrix were detected up to ∼210 °C, above which the spherical domains started to dissolve into the PEB matrix. Finally, the spherical domains were completely dissolved into a homogeneous state at ∼232 °C. The starting and the final dissolution temperatures are referred to as the T_{DDT} and the order-to-disorder transition temperature (T_{ODT}). The LDT was verified by the SAXS results that the higher order diffraction peaks from the bcc lattice disappeared above the T_{LDT}, while particle scattering of spheres due to the intraparticle interference as well as the interparticle interference of spheres in LSO was clearly observed between the T_{LDT} and the T_{DDT}. The spheres in LSO were further elucidated by rheology and TEM observation. It was found that a precipitous decrease in storage modulus (G') and a dramatic change in the Bragg spacing occurred at the same temperature of the T_{LDT}. It was also observed that the slope in the plots of G' versus frequency (ω) and that in the plots of loss modulus (G'') versus ω in the terminal region were two and one, respectively, at temperatures above the T_{LDT}. This is attributed to the fact that because of the absence of the bcc lattice in long-range order, spheres in LSO do not contribute significantly to the shear moduli in the terminal region. Therefore, even if the terminal behavior observed generally for a homogeneous mixture (namely the slopes in the plots of G' versus ω and G'' versus ω are two and one) is exhibited at a temperature, this temperature is not necessarily above the T_{ODT}. The characteristic domain spacing in LSO did not change much with temperature, but it increased between the T_{DDT} and the T_{ODT} due to the dissolution of spheres.

Introduction

Block copolymers exhibit various types of microphase separated structures such as spheres, cylinders, lamellae, and gyroid, due to the segregation between two blocks. These microdomains disappear as the temperature is raised above the transition temperature, which is referred to as the order−disorder transition (ODT) temperature (T_{ODT}). Until now, numerous experimental and theoretical studies have been performed to determine or predict the ODT of block copolymers.[1−13]

Experimental methods to determine the ODT are utilizing small-angle X-ray or neutron scattering (SAXS or SANS),[6,14] rheological measurements,[7−9,11−13] and the depolarized light scattering method.[15,16] Recently, differential scanning calorimetry (DSC) measurement has also been employed.[17−23] Two kinds of rheological methods are relevant to the determination of the ODT: (1) the temperature sweep of the storage modulus (G') experiment, where the T_{ODT} is defined by the temperature where G' drops precipitously,[7−10] and (2) plots of logarithmic G' versus logarithmic loss modulus (G'') (plots of log G' versus log G'') where the T_{ODT} is taken as the threshold temperature, above which these plots are independent of measuring temperatures.[11−13]

For block copolymers with symmetric composition, all methods including DSC measurement give the identical T_{ODT}.[21] However, for a block copolymer with highly asymmetric composition, the T_{ODT} determined by the temperature sweep of the G' experiment is sometimes ∼50 °C less than that obtained by log G' versus log G'' plots.[24,25] The main difference between the two rheological methods is attributed to the existence of the lattice disordering transition (LDT) before reaching the

* To whom all correspondence should be addressed. E-mail jkkim@postech.ac.kr or shin@ipc.kit.ac.jp.

10.1021/ma9902854 CCC: $18.00
Published on Web 09/18/1999

ODT. In other words, the transition temperature determined by the temperature sweep of the G' experiment might correspond to the T_{LDT}, while that determined by log G' versus log G'' plots to the T_{ODT}. At temperatures between the T_{LDT} and the T_{ODT}, log G' versus log G'' plots do not give temperature independence, even though G' and G'' are proportional to ω^2 and ω^1, respectively. Some research groups[8,9,26] have attributed this behavior to the fluctuation effect, which exists in the disordered state above the T_{ODT}. However, in our particular block copolymer with highly asymmetric composition, the spheres (or spherical microdomains) exhibited "liquidlike short-range order" (LSO) above the T_{LDT}, although this ordered state does not belong to any symmetrical space group.

Harkless et al.[27] dealt with the kinetics of the formation of spheres in LDT of a block copolymer as well as the bcc ordering from spheres in LDT when it was quenched from the disordered state. Although they reported that LDT occurred during the transformation of bcc from the disordered state, the T_{LDT} was not discussed in detail. The LDT phenomenon itself was found at first by Hashimoto and co-workers[28] more than 20 years ago. Very recently, Sakamoto and Hashimoto[29] called the spheres (or spherical microdomains) with LSO as "disordered spheres".

In this study, the LDT is defined as the transition temperature from the spheres in a body-centered cubic (bcc) lattice to spheres in LSO and the DDT as the starting temperature of the dissolution of spheres, while the ODT is defined as the temperature above which complete domain dissolution, and thus a homogeneous disordered state, is achieved. It should be mentioned, however, that some research groups[30,31] prefer to assign the LDT as the order-to-disorder transition in their notation and the spheres in LSO as the disordered micelles that are often found at very asymmetric block copolymers.

To have the LDT of a block copolymer, the volume fraction of one block might be very small (say ~0.1). Very recently, Sakamoto et al.[24,25] have extensively studied the existence of the LDT for the mixtures of polystyrene-*block*-polyisoprene-*block*-polystyrene (SIS) copolymers with a weight fraction of a PS block of 0.183 and the neutral solvent of dioctyl phthalate by employing the SAXS method, rheology, and transmission electron microscopy (TEM). The SIS copolymer they have studied exhibited hexagonally packed cylindrical microdomains at lower temperatures and spheres in a bcc lattice at higher temperatures before undergoing the LDT.

The transition point defined by $(\chi N)_t$ for the ODT is raised with increasing degree of asymmetry of the composition. Here, χ is the Flory interaction parameter between two types of segments and N is total number of statistical segments. Thus, a block copolymer with relatively large χ enables us to have the transition at an experimentally accessible temperature, namely a temperature higher than the glass transition (T_g) but lower than the degradation temperature (say 100−250 °C), even though the block copolymer has lower molecular weight. One of candidates for the study on the LDT would be a polystyrene-*block*-poly(ethylene-*co*-but-1-ene)-*block*-polystyrene (SEBS) copolymer. It is known that χ between polystyrene (PS) and poly(ethylene-*co*-but-1-ene) (PEB) is about twice that between PS and polybutadiene (PB) (or between PS and polyisoprene (PI)), when the 1,2-addition in the PEB is about 40 wt %.[32,33] Therefore, to have the T_{ODT} at an experimentally accessible temperature, the molecular weight of an SEBS copolymer having highly asymmetric composition does not need to be higher compared with SI or SIS block copolymers. Easier accessibility of the experimental temperature allows us to distinguish the spheres in LSO from the disordered state. Furthermore, the absence of a double bond in PEB gives much better thermal stability compared with PI or PB; thus, the experiment can be easily carried out up to ~300 °C without concern for thermal degradation or cross-linking problems. It is noted that PI can be thermally degraded or cross-linked under longer exposure times at temperatures higher than ~220 °C.[34]

Since a comprehensive study on the LDT and ODT is not available yet, in this study, the LDT, DDT, and ODT of an SEBS triblock copolymer with a volume fraction of PS block of 0.084 have been investigated by SAXS, TEM, and rheology.

II. Experimental Section

Material. The SEBS-8 sample was kindly supplied by Asashi Chemical Industry. It has a number-average molecular weight (M_n) of 6.7×10^4, volume fraction of the PS block of 0.084, and polydispersity index (M_w/M_n, where M_w denotes the weight-average molecular weight) of 1.04. The content of but-1-ene in the PEB block was 50 mol %, where the ethylene unit represents $-(CH_2)_4-$. Samples subjected to rheological measurement were prepared by first dissolving a predetermined amount of the SEBS-8 in toluene (5 wt %) in the presence of an antioxidant (Irganox 1010; Ciba-Geigy Group) and then slowly evaporating the solvent. After any trace of the solvent was completely removed, the specimen was finally annealed for 24 h at 80 °C that was above T_g (~60 °C) of the PS block. This sample is referred to as the as-cast sample. The as-cast sample was further annealed at two different temperatures, 140 and 150 °C, for 10 h for the SAXS measurements.

Synchrotron Small-Angle X-ray Scattering. The SAXS measurements with synchrotron radiations were conducted at the 3C2 beam line at the Pohang Light Source (PLS), Korea.[35] The primary beam was monochromatized with a couple of Si(111) single crystals at a wavelength of 0.1598 nm (the photon energy of X-rays is 7.76 keV), and then it was focused on a detector plane by a bent cylindrical mirror. A one-dimensional position-sensitive detector (diode-array PSD; Princeton Instruments Inc.; model ST-120) with the distance of each diode of 25 μm was used. The sample thickness was 1 mm. We subtracted the scattering intensity of an empty cell with two pieces of thin polyimide (Kapton) films from that of samples by taking into account the transmittance of X-rays through the samples. A contribution of the thermal diffuse scattering (TDS) arising from the density fluctuations was further subtracted. We approximated that the intensity at the high-q region, where the scattering intensity is independent of q, is identical to the intensity level of TDS. Here, q is the magnitude of the scattering vector, $q = (4\pi/\lambda) \sin(\theta/2)$, where λ and θ are the wavelength of the X-rays and the scattering angle, respectively. The obtained scattering intensities were not converted to absolute units.

Furthermore, to investigate the possibility of the transformation from spheres in LSO to spheres in bcc lattice, the specimen was annealed for various time periods at 150 °C after quenching from a disordered state (240 °C for 10 min). Then, the specimen was quenched into an ice/water mixture, and the SAXS profiles were obtained at room temperature using a goniometer in 5C2 beam line at the PLS. The goniometer in 5C2 beam line allowed us to have SAXS profiles in higher q values (e.g., up to 1.4 nm^{-1}), while the PSD detector in 3C2 beam line gives only up to 0.8 nm^{-1}. The SAXS profiles in higher q values are required to detect the particle scattering of spheres existing between the T_{LDT} and the T_{DDT}, since this

scattering appeared at $q \sim 0.8$ nm^{-1}. Since the scattering intensities at temperatures higher than 210 °C were very weak compared with those at lower temperatures, it is not easy to estimate the maximum intensity and peak position in SAXS profiles. To minimize any error in determining the peak position, in this case, a 2-D CCD camera (Princeton Instruments Inc.; SCX-TE/CCD-1242E) in 1B2 beam line at PLS was employed as a detector, and the circular average of SAXS intensity at a given q was obtained.

Some of the synchrotron SAXS measurements were conducted at the BL-10C beam line of the Photon Factory in the High Energy Accelerator Research Organization, Japan. The light source of this beam line is a bending magnet. The primary beam was monochromatized with a couple of Si(111) crystals at a wavelength of 0.1488 nm (the photon energy of X-rays is 8.33 keV), and then it was focused on a detector plane by a Pt-coated bent cylindrical mirror. A one-dimensional position sensitive proportional counter (PSPC) was used to detect scattering intensities and was set vertically at a position 1.9 m apart from the sample position. We subtracted the scattering intensity of an empty cell with two pieces of thin poly(ethylene terephthalate) films from that of samples by taking into account the transmittance of X-rays through the samples, and the TDS was also corrected for.

Transmission Electron Microscopy (TEM). The microdomain structures of the SEBS-8 annealed at various temperatures were investigated by TEM. Ultrathin sectioning was performed by using a Leica Ultracut UCT microtomer at a cryogenic environment. Then, a Hitachi H-600A transmission electron microscope operated at 75 kV was used to obtain micrographs of the specimens stained with ruthenium tetraoxide for ~10 h. Because of selective staining, PS domains appeared black and PEB matrix white in TEM micrographs.

Rheological Properties. Using an Advanced Rheometrics Expansion System (ARES) with parallel plates of 25 mm diameter, a dynamic temperature sweep experiment and a frequency sweep experiment at each temperature during heating and temperature jumping tests were performed. A dynamic temperature sweep experiment was done under isochronal conditions with increasing temperature from 130 to 250 °C. Before heating, the sample was annealed at 130 °C for 10 h. The heating rate was 0.5 °C/min, and the strain amplitude (γ_0) and the angular frequency (ω) were 0.05 and 0.1 rad/s, respectively. This condition lies in a linear viscoelastic regime. It was found that the linear viscoelasticity was observed up to $\gamma_0 = 0.065$ at 130 °C and $\omega = 0.1$ rad/s. Of course, with increasing temperature, the linear viscoelastic regime for γ_0 was greatly expanded; for instance, it was observed up to $\gamma_0 = 0.20$ at 160 °C and $\omega = 0.1$ rad/s. To study the kinetics of the LSO state, the temperature quench experiment was conducted from 250 °C in a disordered state to 150 °C corresponding to the spheres in LSO. The sample temperature was stabilized at 150 °C within 2 min in the rheometer after the sample was quenched from 250 °C. The time evolution in G' at 150 °C under $\gamma_0 = 0.05$ and $\omega = 0.1$ rad/s was observed up to 1 week.

III. Results and Discussion

Figure 1 shows the SAXS profiles (logarithm of the scattering intensity ($I(q)$) versus q) measured at room temperature for the as-cast and the samples annealed at 140 and 150 °C for 10 h followed by quenching into an ice/water mixture. The SAXS profiles were measured at the Photon Factory, Japan. To avoid overlaps of the SAXS profiles, these are vertically shifted. It can be seen in Figure 1 that the microdomain morphologies for the as-cast sample and the sample annealed at 150 °C are very difficult to determine due to the absence of the higher order peaks. However, in addition to a distinct first-order peak and a first-order particle scattering peak marked by a thick arrow at $q \sim 0.76$ nm^{-1}, a broad shoulder marked by a thin arrow appears at $q = 0.42$ and 0.45 nm^{-1} for the as-cast sample and the annealed

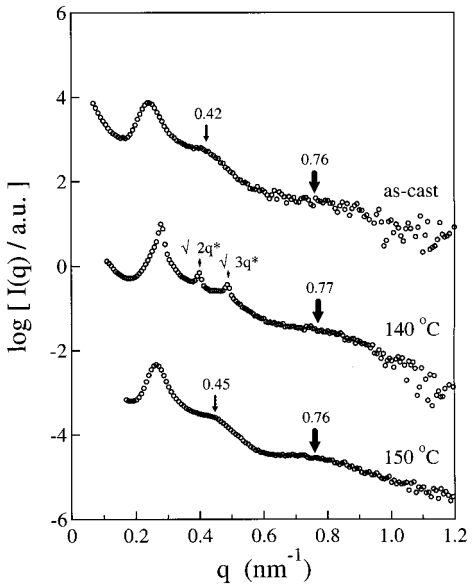

Figure 1. SAXS profiles measured at room temperature for the as-cast sample and the samples annealed at 140 and 150 °C for 10 h. The thick and thin arrows represent the first-order particle scattering peak and the tail of the zeroth-order particle scattering peak from spheres in LSO.

sample at 150 °C, respectively. This broad shoulder was due to the intraparticle interference (namely, the tail of the zeroth-order particle scattering peak) of spheres in LSO, as will be discussed in detail later. On the other hand, the sample annealed at 140 °C for 10 h clearly shows higher order peaks at $\sqrt{2}q_m$ and $\sqrt{3}q_m$, where q_m is the q value of the first-order peak, which implies that this sample has spherical microdomains packed in the bcc lattice. It is noted that spherical microdomains packed in a simple cubic (SC) also exhibit higher order peaks at $\sqrt{2}q_m$ and $\sqrt{3}q_m$. However, the determination of microdomains between the two can be easily done, when experimental volume fraction of PS (ϕ_{PS}) is compared with the predicted one on the basis of the first-order lattice scattering and the first-order particle scattering peak positions. For the bcc microdomain, ϕ_{PS} is given by[36]

$$\phi_{PS} = \frac{\sqrt{8}\pi}{3}\left(\frac{\bar{R}}{d}\right)^3 \quad (1)$$

where $\bar{R}$ is the average radius of PS sphere and given by $5.764/q_{max}$ where q_{max} is the first-order particle scattering peak position occurring at 0.77 nm^{-1} (marked by a thick arrow). The d is the domain spacing given by $2\pi/q_m$ where q_m is the maximum peak position occurring at 0.27 nm^{-1}. Using these values, the calculated $\bar{R}$ for bcc microdomains is 7.7 nm and ϕ_{PS} is 0.095. Since predicted ϕ_{PS} for the SC microdomain is $2^{1/2}$ times larger than that for bcc microdomain, it was estimated to be 0.0134. Comparing these two with experimental value, it is concluded that SEBS-8 has bcc microdomains at 140 °C.

From the results, we conclude that a transition occurred between 140 and 150 °C. However, this transition should not be considered as the ODT, because the SAXS profile at 150 °C is completely different from that in a disordered state. For instance, the broad higher order peak marked by a thick arrow near 0.76 nm^{-1} is clearly observed in the SAXS profile at 150 °C, which corresponds to the first-order particle scattering peak from spheres. On the basis of the SAXS results, the

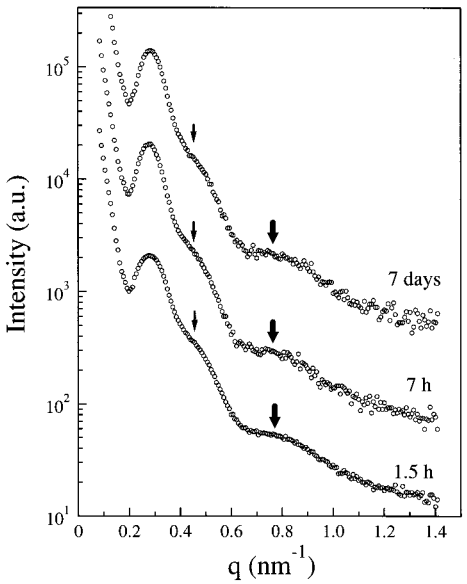

Figure 2. SAXS profiles measured at room temperature after the specimen was socked for 15 min at 240 °C followed by quenched to 150 °C and annealed at this temperature for various time periods. Finally, it was quenched into an ice/water mixture. The thick and thin arrows represent the first-order particle scattering peak and the tail of the zeroth-order particle scattering peak from spheres in LSO.

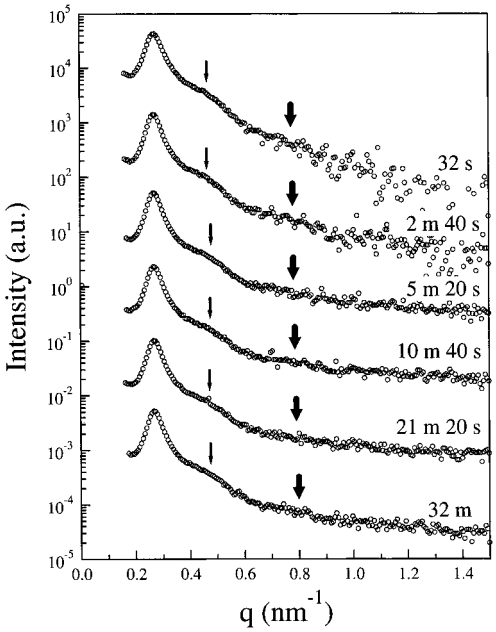

Figure 3. SAXS profiles with time after the specimen was quenched to 150 °C from 240 °C. Before quenching, the specimen was annealed for 1.5 h at 240 °C. The thick and thin arrows represent the first-order particle scattering peak and the tail of the zeroth-order particle scattering peak from spheres in LSO.

spheres in LSO exist at 150 °C. Therefore, we can conclude that the above transition was assigned as the LDT. The poor ordering of spheres into the bcc lattice for the as-cast sample is because the time required for sphere ordering was not sufficiently long before the PS domains were vitrified at the casting (room) temperature due to an increase of polymer concentration in the casting solution.

To find the effect of thermal history on the SAXS profiles, the sample was quenched from a homogeneous state (240 °C for 10 min) to 150 °C, followed by annealing at 150 °C for various times periods up to 3 weeks. Finally, it was quenched into ice/water. Figure 2 gives the SAXS profiles measured at room temperature for the annealed sample at 150 °C after quenching from disordered state. The SAXS profiles were measured at 5C2 beam line in PLS, Korea. It is seen that the profiles are essentially the same regardless of annealing times up to 3 weeks, although the SAXS profiles for only up to 7 days are shown. Furthermore, the SAXS profiles in Figure 2 are almost the same as those in Figure 1, even though SAXS profiles are measured in two places, Korea and Japan. Namely, in addition to a distinct first-order peak at $q = 0.28$ nm^{-1}, a broad shoulder marked by a thin arrow appeared at $q = 0.45$ nm^{-1}, corresponding to the tail of the zeroth-order particle scattering peak of spheres in LSO.[37] Also, the broad higher order peak at $q \sim 0.77$ nm^{-1} marked by a thick arrow in Figure 2 corresponds to the first-order particle scattering peak from spheres, suggesting that the spheres in LSO exist at 150 °C.

However, the SAXS profiles given in Figures 1 and 2 are not measured at 150 °C but measured at room temperature after the specimen was quenched to ice/water. Thus, it is not completely excluded that even if spheres have not existed at 150 °C, spheres in LSO might be formed during the quenching process from 150 °C to ice/water. To investigate this effect, we prepared a sample annealed at 240 °C for 15 min (namely above ODT, which will be discussed later) followed by a rapid quench into ice/water. Interestingly, the SAXS profiles of this sample are almost the same as those annealed at 150 °C. This implies that even though the specimen is indeed in the disordered state, it is almost impossible to fix the morphology in the disordered state during a very rapid quenching. Therefore, the SAXS profiles of a specimen measured at room temperature should be carefully interpreted, even if the specimen was annealed at a specific temperature for a long time.

Thus, we performed another SAXS measurement for a specimen annealed at 155 °C for 1.5 h in the heating block and found that the broad peak near $q \sim 0.77$ nm^{-1} was clearly observed. Figure 3 gives the time-resolved SAXS profiles measured after the specimen was placed from one heating block maintained at 240 °C to the other at 150 °C. It is noted that due to very large temperature difference, it took about 4 min for the sample temperature to be equilibrated. It is seen in Figure 3 that a broad peak marked as a thick arrow at $q \sim 0.77$ nm^{-1} corresponding to the first-order particle scattering peak from spheres in LSO as well as the first-order peak at 0.27 nm^{-1} developed in less than 30 s. Furthermore, a shoulder marked as a thin arrow corresponding to the tail of zeroth-order particle scattering peak of spheres in LSO was observed at 0.45 nm^{-1}. However, the long-range lattice order was not developed. Therefore, on the basis of results given in Figures 1−3, we concluded that a broad first-order particle scattering peak as well as a shoulder seen in Figures 1 and 2 is not due to quenching effect but to the existence of spheres in LSO.

To investigate in detail the transition and morphological change with temperature for SEBS-8, we performed a SAXS measurement during heating at a rate of 0.5 °C/min and an exposure time of 30 s. The specimen was prepared by annealing at 140 °C for 10 h and quenching into an ice/water mixture. Then, the specimen was soaked at 136 °C for 30 min before the SAXS measurement. One argues that the heating rate

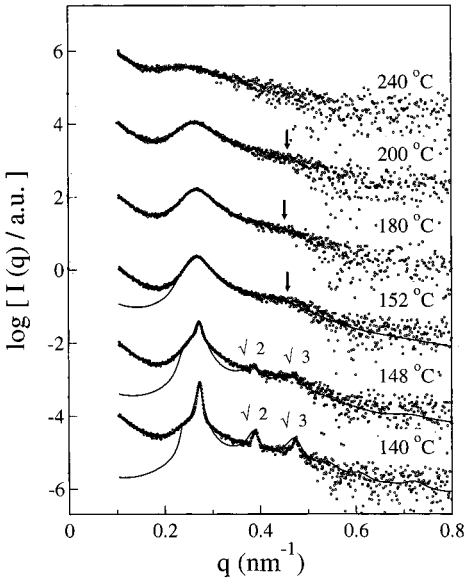

Figure 4. SAXS profiles at various temperatures obtained during the heating at a rate of 0.5 °C/min. The solid curve at each sample was calculated from the paracrystal theory that was described in the Appendix. Thin arrow represents the tail of the zeroth-order particle scattering peak from spheres in LSO.

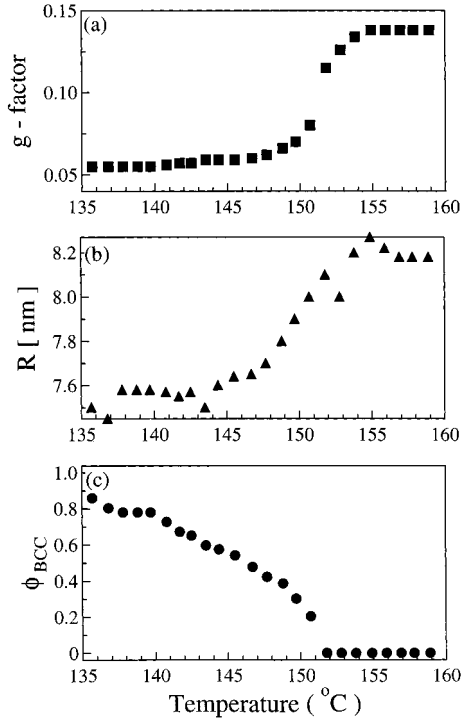

Figure 5. Plots of (a) g-factor, (b) $\bar{R}$, and (c) fraction of the bcc region (ϕ_{bcc}) versus temperature near the T_{LDT}.

of 0.5 °C/min might not be too slow to assume that SAXS profiles obtained at each temperature are indeed in an equilibrium. Thus, SAXS experiments were carried out after annealing for 15 min at several temperatures (140−240 °C) without quenching. We found that SAXS profiles are essentially the same as those given in Figure 4, as evident in Figure 6 where open symbols are obtained after annealing for 15 min at a temperature. This is because the relaxation time of SEBS-8 at these temperatures is estimated to be very short. The longest relaxation time (τ) of a polymer in the molten state is estimated by $12\eta_0/(\pi^2 G_N^o)$.[40] The plateau modulus

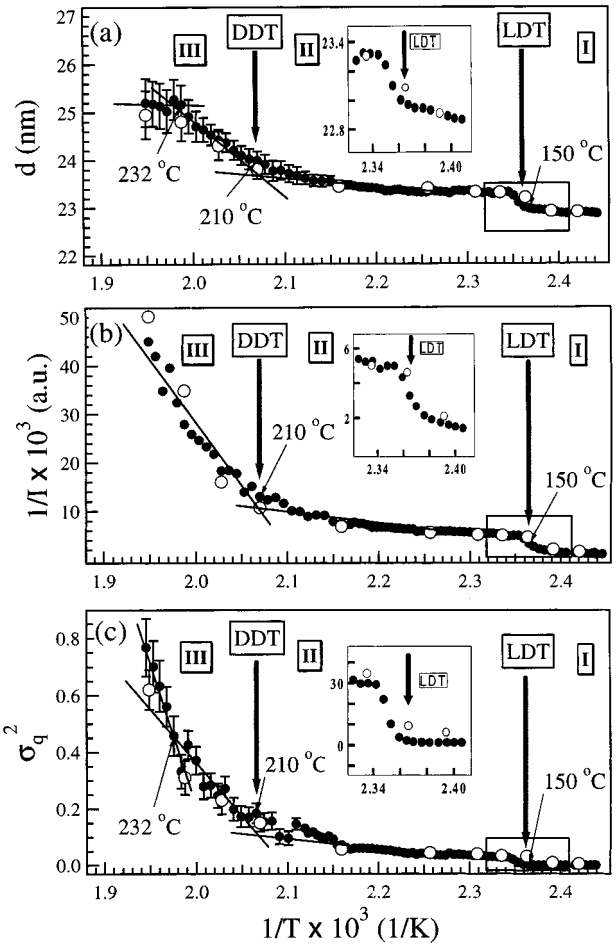

Figure 6. Plots of (a) the Bragg spacing ($d = 2\pi/q_m$), (b) $1/I(q_m)$, and (c) the square of the full width at the half-maximum intensity (fwhm; (σ_q^2)) versus $1/T$ for the first-order peak. The inset in each curve highlights a dramatic change of each variable near the LDT.

Table 1. Structure Parameters Used in the Model Calculation of SAXS Profiles

sample (°C)	f_{bcc}	g-factor	d (nm)	$\bar{R}$ (nm)	σ_R (nm)	t_I (nm)	ϕ_A
140	0.78	0.055	22.9	7.6	1.3	1.30	0.11
148	0.30	0.07	23.1	7.9	1.2	1.30	0.12
152	0	0.134	23.1	8.2	1.5	1.30	0.13
158	0	0.138	23.1	8.2	1.4	1.40	0.13

(G_N^o) of SEBS-8 would be very similar to that (9×10^5 Pa)[41] of the PEB block due to the small amount of PS block. Since η_0 at 150 °C was about 1.5×10^4 Pa s as shown later, the relaxation time at 150 °C would be as small as 0.02 s. Also, at higher temperatures, the relaxation time is more reduced due to smaller viscosity. Therefore, SAXS profiles at several temperatures obtained during heating at a heating rate of 0.5 °C/min, as shown in Figure 4, represent almost equilibrium properties.

The solid curves given in Figure 4 are the scattering functions calculated using the paracrystal theory[42−44] which is described in detail in the Appendix, and the parameters employed in the model calculations for each specimen are summarized in Table 1. It can be seen that the agreement between the experimental and calculated SAXS profiles is satisfactory for all samples when we take into account the considerably low scattering intensities in the range $q > 0.5$ nm^{-1}. Although the

calculated value of the volume fraction of PS (ϕ_{PS}) is slightly larger than that (0.084) obtained by NMR, this difference is not significant. The predictions for SAXS profiles above 240 °C were not included due to the absence of higher order peaks.

It can be seen in Figure 4 that higher order peaks corresponding to $\sqrt{2}q_m$ and $\sqrt{3}q_m$ are clearly observed at 140 °C. However, it is of interest to note that the first-order peak in the SAXS profile at 140 °C would be the superposition of a sharp scattering peak from the bcc lattice and a broad scattering peak from interparticle interference of spheres in LSO. This is consistent with the fact that the bcc lattice and the LSO coexisted at 140 °C, which was determined by TEM as shown later. We calculated the fraction of bcc lattice phase, f_{bcc}, at a temperature between 135 and 150 °C by the best fitting for the SAXS profile at each temperature, when the first-order peak was assumed to be expressed with a linear combination of a sharp scattering peak from the bcc lattice and a broad one from a more distorted bcc lattice in the LSO region. Notice that the bcc lattice peak was obtained from the best fitting with the contribution of the LSO regions using the paracrystal theory. Furthermore, the assumption was employed that spheres in LSO did not depend on temperatures ranging from 135 to 150 °C. Using this procedure, we determined the f_{bcc} at 140 °C to be 0.78. Namely, at this temperature 22% would be LSO phase. However, the f_{bcc} at 148 °C was 0.30, which implies that the bcc lattice peaks started to disappear.

Interestingly, a broad shoulder marked by a thin arrow at $q \sim 0.45$ nm^{-1} was clearly observed at temperatures higher than 150 ± 0.5 °C, which is essentially the same as SAXS profile for the sample annealed at 150 °C given in Figure 1. This broad shoulder was due to the intraparticle interference of spheres in LSO. We found that this broad shoulder was observed up to ~210 °C although the exact temperature corresponding to the disappearance of this shoulder was rather difficult to determine. The SAXS profile at 240 °C seemed to correspond to a completely disordered state, because of very low intensity and a broad first-order peak without any shoulder in the high q region.

The T_{LDT} was determined from the plots of g-factor, the average radius of spheres ($\bar{R}$), and the f_{bcc} versus temperature, as shown in Figure 5. Here, the paracrystalline distortion factor, g, is defined by $\Delta d/d$ where Δd is the standard deviation of d (Bragg spacing) due to the distortion. The T_{LDT} was determined to be 150 ± 0.5 °C, from the temperature changes of these parameters. The abrupt increase of the g-factor at the T_{LDT} means that packing regularity became poorer as the bcc lattice phase proceeded to transform into LSO. The value of g-factor below the T_{LDT} was calculated by the best fitting of the SAXS profile in the bcc region with the contribution of the LSO region.

Figure 6 gives the plots of the d, the inverse of the first-order peak intensity ($1/I(q_m)$), and the square of the full width at the half-maximum (fwhm; (σ_q^2)) for the first-order peak versus ($1/T$). Open symbols at each part were obtained from SAXS profiles when a specimen was annealed for 15 min at a specific temperature. It is seen that the SAXS profiles obtained during heating at a rate of 0.5 °C/min are essentially the same as those obtained after annealing for 15 min at a specific temperature. The d in Figure 6a stands for the Bragg spacing in the bcc state, but it means the most probable spacing in the LSO and the dominant wavelength of the concentration fluctuation in the disordered state. On the basis of the slope changes given in Figure 6a−c, three different regimes can be considered: regime I corresponding to the spheres in the bcc lattice, regime II to spheres in LSO, and regime III to the dissolution of spheres.

The transition from regime I to regime II was easily assigned to the LDT, and this was consistent with the results given in Figure 5. Sharp increases in the d, $1/I(q_m)$, and σ_q^2 were detected upon the LDT, as shown in the insert of each curve. Furthermore, the G' decreased very rapidly upon the LDT, which will be corroborated later. The smaller d ($=2\pi/q_m$) and the smaller radius of the spheres (see Table 1) in the bcc lattice compared with those in the LSO state might have resulted from the constraint of the bcc lattice; namely, spheres in a regular bcc lattice are slightly collapsed compared with spheres in LSO. This was also reported for an SIS copolymer by Sakamoto et al.,[25] who attributed this increase in the d during the LDT to the broken symmetry from spheres in the bcc lattice to spheres in LSO. The d of a block copolymer with cylindrical microdomains and lamellae usually decreases as temperature approaches T_{ODT} of the block copolymer, because the degree of the chain stretching in those microdomains decreases with increasing temperature. But, because of the existence of spheres, the bcc lattice in this study does not become a completely disordered state above the LDT, which implies that the decrease in the chain stretching does not necessarily happen upon the LDT. Semenov[45] and Olvera de la Cruz[46] also showed that the d decreases with decreasing temperature from a disordered state to bcc microdomains. Although she[46] did not include the effect of the LDT on the d during the disordering of the bcc lattice, it seems that the disordering of the bcc lattice to a disordered state would be different compared with that of cylindrical microdomains and lamellae.

Interestingly, as shown in Figure 6b,c, with increasing temperature $1/I(q_m)$ and σ_q^2 in the regime II increased very little, even if the degree of distortion of the bcc lattice in a short range increased with increasing temperature. Furthermore, the d became almost constant; thus, the most probable distance between spheres in LSO did not change. Little change in the d with increasing temperature in regime II is inconsistent with results for SI diblock copolymer[39] and the mixture of SIS triblock copolymer and DOP.[25] Although the reason is not clear at the present time, the bridge conformation in the bulk triblock copolymer might play an important role. At a temperature of ~210 °C, the slopes in all plots of d, $1/I(q_m)$, and σ_q^2 versus $1/T$ changed significantly. We speculated that the PS spherical domains (or disordered spheres) started to dissolve into PEB matrix at this temperature. We found that a shoulder at 0.45 nm^{-1} from the tail of the zeroth-order particle scattering peak of spheres in LSO disappeared at temperatures higher than ~210 °C, although the assignment of this temperature was not easy due to the weak intensity for the shoulder. We assigned the temperature that delineates regime II from regime III as the T_{DDT} (the onset of the domain dissolution transition). Thus, regime III corresponds to the domain dissolution regime where spheres in LSO dissolve gradually into the PEB matrix and become a disordered state. Interestingly, the d in regime III increased with increasing temperature before it seemed to level off at temperatures higher than ~232

°C. It is not clear why the d increased with increasing temperature in temperature region. But, it might be attributed to the decrease in the population of PS spheres, as the domain dissolution proceeded. Previously, Sakamoto et al.[25] reported a similar behavior, but they employed mixture of SIS and dioctyl phthalate (DOP) where an osmotic pressure of DOP would increase d in this regime.

Even though the circular average of the 2-D scattering patterns at a given q was employed, the exact peak position and intensity of SAXS profiles are very difficult to determine at higher temperatures in regime III because of weak scattering intensity (see SAXS profiles at 240 °C in Figure 4). But, as shown in Figure 6a, the d seems to be constant at temperatures higher than ~232 °C. Furthermore, the slope in plots of σ_q^2 versus $1/T$ changed greatly at ~232 °C. Therefore, it might be possible to consider that the order-to-disorder transition temperature (T_{ODT}) was ~232 °C, although the exact determination is very hard. Here, we defined the T_{ODT} as the transition temperature from spheres in LSO to the disordered (or homogeneous) state. Previously, Sakamoto et al.[25] determined the T_{ODT} (or T_D in their terminology) as the temperature where the slope in plots of the d and σ_q^2 changed significantly. When their argument is used, we can determine the T_{ODT} of ~210 °C. This temperature gap (~22 °C) for the complete dissolution of disordered spheres is not unexpected due to the slow dynamic process of the migration of individual block chains.[29]

Figure 7 gives TEM micrographs for the as-cast sample and the sample annealed at 150 °C for 10 h, and Figure 8 gives TEM micrographs for the samples annealed at 130 and 140 °C for 10 h. The dark region corresponds to PS domains stained with ruthenium tetraoxide, and the bright matrix is the unstained PEB phase. PS spheres were observed for all samples. The lattice-disordered state was confirmed for the as-cast sample and the sample annealed at 150 °C for 10 h as shown in Figure 7, whereas well-ordered spheres were manifested for the samples annealed at 130 and 140 °C for 10 h as shown in Figure 8. For the sample annealed at 130 °C for 10 h, the TEM image as shown in Figure 8a consisted of three grains (A, B, and C) and one lattice-disordered region (D). The projection from a ⟨111⟩ direction was observed in the grains A and B, whereas the projection from a ⟨100⟩ direction was clearly seen in the grain C. The grain boundary among each grain (A, B, and C) was well manifested. On the other hand, Figure 8b for the sample annealed at 140 °C for 10 h exhibited two distinct grains: One (grain A) exhibited the projection from a ⟨111⟩ direction of the bcc lattice, and the other (grain E) was poorly ordered. However, even if the grain E in Figure 8b seemed partly lattice-disordered, this image differed significantly from the lattice-disordered state as shown in Figure 7a,b.

It should be mentioned that TEM images for a sample annealed at temperatures higher than T_{DDT} (230 °C) for 30 min followed by quenching to ice/water was very similar to that of a specimen annealed at 150 °C for 1 h followed by quenching to ice/water. Furthermore, we found that SAXS profiles of the former specimen were almost the same as those of the latter. This implies that even though the specimen is indeed in the disordered state, it is almost impossible to fix the morphology in the disordered state during a very rapid quenching. Thus, in this study, instead of taking TEM images, an in-situ SAXS experiment was carried out after the specimen was quenched from 240 °C to temperatures larger than T_{LDT}, and the results are given in Figure 3.

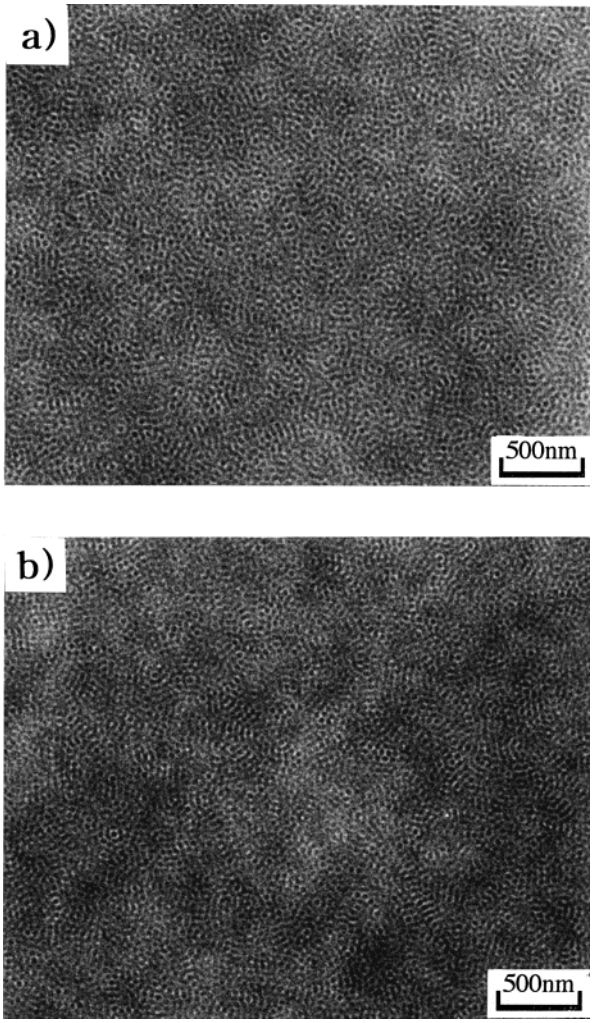

Figure 7. TEM micrographs for (a) the as-cast sample and (b) the sample annealed at 150 °C for 10 h.

Figure 9 gives temperature sweep experiments of G' of SEBS-8 at ω of 0.1 rad/s and γ_0 of 0.05 during heating at a rate of 0.5 °C/min after the sample was annealed at 130 °C for 10 h. From the TEM image given in Figure 8b, spheres in the bcc lattice are clearly seen at this annealing condition. Also, in Figure 9 is shown a cooling scan of G' at a rate of 0.5 °C/min after the sample was maintained at 250 °C for 10 min. It can be seen that during heating G' decreased very sharply at ~150 °C. However, when the sample was annealed at 80 °C for 24 h, a sharp decrease in G' similar to that observed during the heating in Figure 9 was not observed at ~150 °C; rather, the slope of the plots of G' versus temperature was changed at this temperature. This result again suggests that the well-ordered bcc state for a block copolymer having a highly asymmetric composition could not be observed without a proper annealing condition. Furthermore, the increase in G' during the cooling was not evident compared with the decrease in G' during the heating, because the formation of the long-range order by cooling takes a much longer time than the disruption of long-range order by heating.[25,47]

When the T_{ODT} is defined as the temperature at which a precipitous decrease in G' is observed, the T_{ODT} would

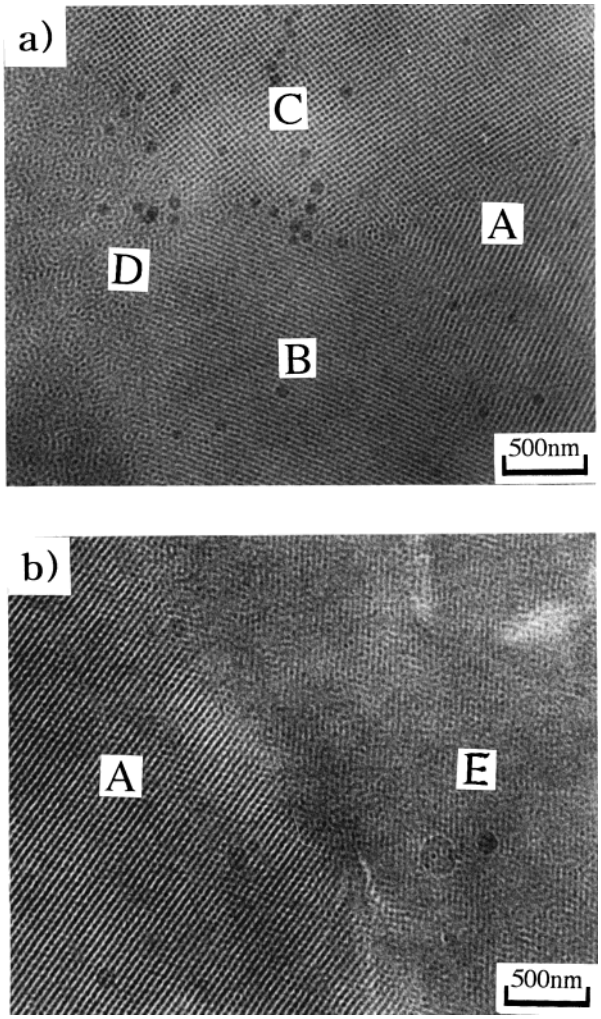

Figure 8. TEM micrographs for the samples annealed at (a) 130 and (b) 140 °C for 10 h. Here, grains A and B were viewed from a ⟨111⟩ direction, whereas grain C was viewed from a ⟨100⟩ direction. Also, grain D corresponding to a lattice-disordered region was observed in part a, whereas poorly ordered grain E was observed in part b.

be 150 °C. However, this definition must be reserved for block copolymers with highly asymmetric compositions[12,13,24,25] since in these block copolymers spheres in LSO were detected at temperatures higher than the T_{ODT} defined above. Schwab and Stühn[39] showed that for an asymmetric SI copolymer (volume fraction of PS is 0.11) spheres in LSO existed between bcc and the disordered state, which was deduced from the existence of a higher order peak in the SAXS profiles due to particle scattering of spheres. Harkless et al.[27] also reported that when temperature was quenched from the disordered state to the bcc regime, the polystyrene-*block*-polybutadiene copolymer with the solvent of C-14 stayed at LSO state before complete transformation to the bcc state. Thus, the above-mentioned rheological criterion[7−9,26,48] as the definition of the T_{ODT} should be carefully employed for highly asymmetric block copolymers without SAXS profiles, allowing one to confirm whether the spherical microdomains indeed exist or not. Otherwise, the T_{LDT} delineating one regime corresponding to spheres in LSO from the other regime corresponding to spheres in bcc lattice can be erroneously taken as the T_{ODT}.

On the other hand, another rheological criterion that the T_{ODT} is taken as the threshold temperature, above

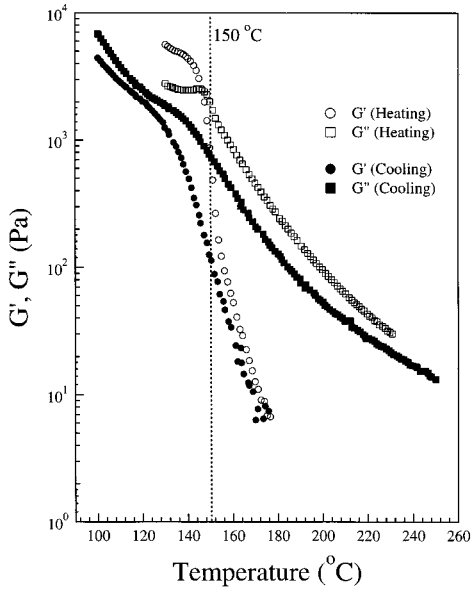

Figure 9. Temperature sweep experiment of G' of SEBS-8 at ω of 0.1 rad/s and γ_0 of 0.05 during heating (open symbols) after the sample was annealed at 130 °C for 10 h and during a cooling scan (closed symbols) after the sample was annealed at 250 °C for 10 min. Both heating and cooling rates are 0.5 °C/min.

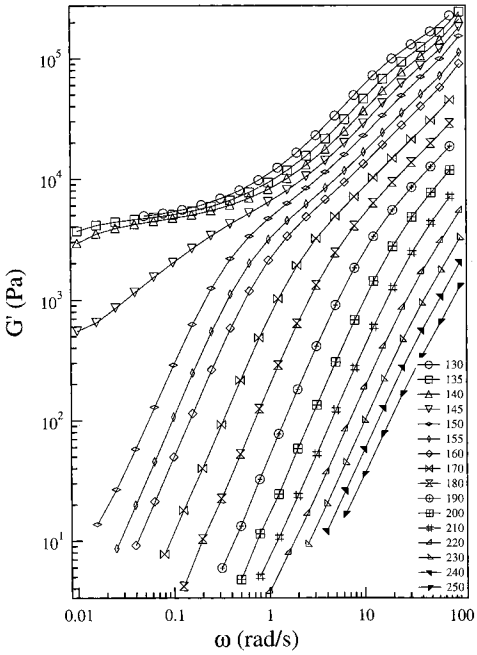

Figure 10. Log G' versus log ω at various temperatures with γ_0 of 0.05. These are obtained during the heating of the sample and soaking for 30 min at each temperature.

which plots of log G' versus log G'' show temperature independence, becomes a powerful one to determine the T_{ODT} for highly asymmetric block copolymers.[12,13,24,25] Figures 10 and 11 give plots of log G' versus log ω and log G'' versus log ω at various temperatures, respectively. Before the measurement the sample was annealed at 130 °C for 10 h, and the sample was soaked for 30 min at each measuring temperature. At temperatures lower than 140 °C, G' at lower ω changes very little with frequency; namely, the slope of log G' versus log ω plots is almost zero, which is typical behavior for block copolymers with microdomains of three-dimensional structures such as bcc or gyroid microdomains.[49,50]

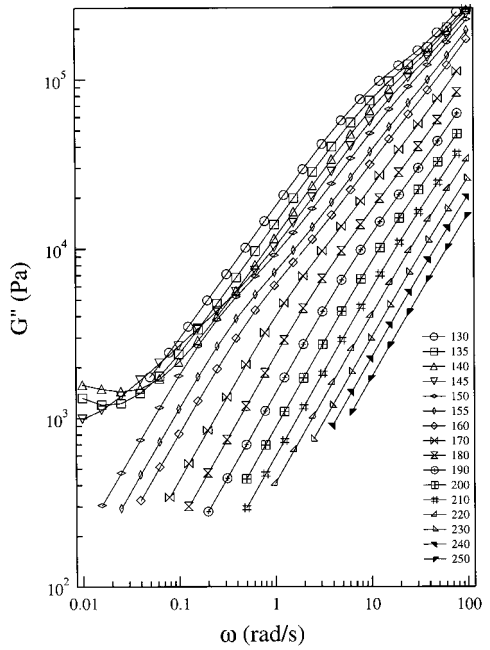

Figure 11. Log G'' versus log ω at various temperatures with γ_0 of 0.05. These are obtained during the heating of the sample and soaking for 30 min at each temperature.

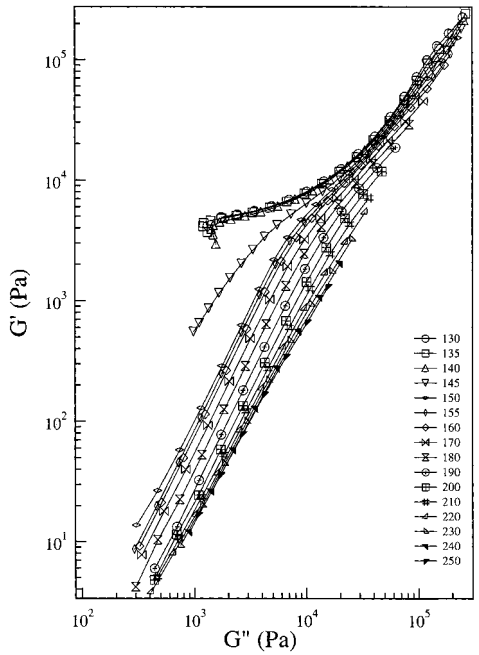

Figure 12. Log G' versus log G'' at various temperatures.

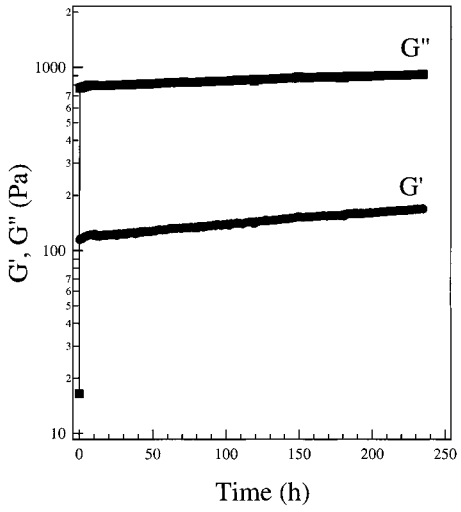

Figure 13. Time evolution of G' and G'' at 150 °C under $\gamma_0 = 0.05$ and $\omega = 0.1$ rad/s after the temperature was quenched from 250 to 150 °C. Before quenching, the specimen was annealed for 10 min at 250 °C.

Similar behavior was observed for G''; that is, G'' at lower ω did not decrease with increasing temperature when measuring temperature was lower than 145 °C. At 145 °C, G' dropped but still had a slope less than two. We speculated that bcc spheres were still present at this temperature, while most bcc lattices already lose the solidlike long-range orders (namely spheres in LSO became the majority). This is consistent with the result given in Figure 4 where $\sqrt{2}q_m$ and $\sqrt{3}q_m$ peaks were still observed at 148 °C. Finally, at temperatures higher than 150 °C, the slope of log G' versus log ω plots becomes two and the slope of log G'' versus log ω plots becomes one.

On the basis of these results, plots of log G' versus log G'' are given in Figure 12. Interestingly, these plots became independent of temperatures higher than 230 °C and the slope became two, although a sharp drop in G' was observed between 145 and 150 °C. If the slope of two in plots of log G' versus log G'' would represent the disordered state, the T_{ODT} might be taken as 150 °C. However, in this situation the difference between the T_{ODT} and the temperature above which a complete disordered state was obtained would be as much as 80 °C, since temperature independence of plots of log G' versus log G'' was first achieved at 230 °C. On the basis of the SAXS results described above, the parallel displacement in the plots of log G' versus log G'' with temperature, even though the slope is identical to two, is not attributed to fluctuation effects in the disordered state but to the existence of spheres in LSO.

At temperatures above 150 °C, because there are no three-dimensional bcc lattices in a long range, the block copolymer behaves like a molten liquid even if PS spheres in LSO exist in the PEB matrix. Interestingly, the second plateau modulus in G' near 3×10^3 Pa is clearly seen at temperatures between 150 and 170 °C, as shown in Figure 10. This behavior is also found for immiscible polymer blends with dispersed domains and explained by the emulsion model.[51,52] Although the emulsion model can predict the size of dispersed domains in an immiscible polymer blend, we do not try to estimate the domain size of the spheres because the emulsion model might not be applicable to the block copolymer. On the basis of the above results, we conclude that the T_{ODT} of SEBS-8 was determined to be ~230 °C since the plots of log G' versus log G'' are completely temperature independent at temperatures higher than 230 °C. This result is consistent with the above SAXS results. It should be pointed out, however, that the good agreement between SAXS and rheological results to determine the T_{ODT} might be fortuitous, once two different methods (SAXS versus rheology) and experimental error are considered. Even though we consider this possibility, the T_{ODT} was much higher than the T_{LDT} (as high as ~80 °C).

Figure 13 gives time evolution of G' and G'' at 150 °C under $\gamma_0 = 0.05$ and $\omega = 0.1$ rad/s after the temperature was quenched from 250 °C (in the disordered state) to

150 °C. Interestingly, G' and G'' were very slowly increased as the time elapsed. If the temperature of 150 °C had been in the disordered state, the moduli would not have increased at all with time. However, the very slow increase in the moduli with time as shown in Figure 13 suggests that there existed spheres in LSO, and the order of the packing in spheres might develop with time. Because the modulus should increase dramatically during the formation of the bcc lattice, we concluded that the spheres in LSO were not transformed into the bcc lattice even when the sample was annealed at this temperature for up to 1 week.

Before closing this work, it is argued whether the transition temperatures are observed by DSC measurement. We previously reported the existence of the endothermic peak of the T_{ODT} of a block copolymer with a symmetric composition, thus having a lamellar microdomain.[21] However, any discernible peak near T_{LDT}, T_{DDT}, and T_{ODT} was not observed in DSC thermogram for SEBS-8. This is due to very asymmetric composition of SEBS-8 ($\phi_{PS} = 0.084$); thus, the endothermic peak at the T_{ODT} would be very small, if any. Thus, it is considered that a conventional DSC such as Perkin-Elmer DSC-7 series does not detect the T_{ODT} for a block copolymer with a highly asymmetric composition.

IV. Conclusions

In this study, we have shown that the LDT, DDT, and ODT were determined by SAXS, TEM, and rheology, for the SEBS-8 copolymer with a volume fraction of PS block of 0.084. The SEBS-8 sample formed spherical microdomains packed in a bcc lattice at lower temperatures and underwent the LDT at 150 ± 0.5 °C. The determination of the LDT was straightforward since SAXS profiles and rheological properties changed dramatically at this temperature. Above this temperature, the distorted bcc or spheres in LSO with a relatively narrow interface between PS domain and PEB matrix were detected up to ~210 °C. This temperature was referred to as the T_{DDT}, which was determined by the disappearance of the contribution of the particle scattering of spheres in the SAXS profiles. The T_{DDT} was slightly different from the complete domain dissolution temperature (or T_{ODT}) of ~232 °C, which was obtained by the temperature independence in plots of log G' versus log G'' and by the change in the slope of plots of the d and σ_q^2 versus $1/T$. We clearly showed that the fact that the slopes in plots of G' and G'' versus frequency in the terminal region are two and one, respectively, at temperatures between T_{LDT} and T_{ODT} were due not to the so-called fluctuation effect existing in the disordered states, but to the existence of spheres in LSO, which contributes to viscoelasticity, although not large.

Acknowledgment. We acknowledge Professors C. D. Han at the U. of Akron, T. Lodge at the U. of Minnesota, N. Balsara at the Polytechnic U., and G. Floudas at the FORTH for constructive suggestion on the LDT and ODT. This work was carried out under the Korean−Japan joint research program (986-0300-004-2) supported by KOSEF and JSPS and supported in part by POSTECH/BSRI special fund (1999). Synchrotron SAXS experiments were performed at the PLS (3C2, 5C2, and 1B2 beam lines) in Korea, which was supported by Ministry of Science and Technology (MOST) and POSCO, as well as at the Photon Factory (Proposal No. 97G230) in Japan. S.S. acknowledges the Grant-in-Aid (08751048) from Japan Ministry of Education, Science, Culture, and Sports.

Appendix

According to the paracrystal theory, $I(q)$ for microphase-separated block copolymers can be formulated as follows:[43,44]

$$I(q) = \langle |f^2(q)| \rangle - |\langle f(q) \rangle|^2 + |\langle f(q) \rangle|^2 Z(q) \quad \text{(A1)}$$

where $f(q)$ and $Z(q)$ denote the scattering amplitude due to the intraparticle interference and the scattering intensity due to the interparticle interference, respectively. Hereafter, $f(q)$ and $Z(q)$ are referred to as the particle and the lattice factor, respectively. In eq A1, $\langle x \rangle$ is the average of the quantity of x. $f(q)$ for a spherical particle with its radius, R, can be given by the Fourier transformation of the variation of the electron density in the real space and reads

$$f(q) = 3A_e \Delta\rho V \frac{\sin(qR) - qR\cos(qR)}{(qR)^3} \exp\left(-\frac{\sigma_s^2 q^2}{2}\right) \quad \text{(A2)}$$

where A_e is the scattering amplitude of Thomson scattering (scattering from an electron), $\Delta\rho$ ($= |\rho_A - \rho_B|$) is the difference in the electron density between the sphere and the matrix, V is the volume of the spheres, and σ_s is a parameter characterizing the variation of the (electron) density in the interfacial region. The characteristic thickness of the interface, t_I ($= \Delta\rho/|d\rho(z)/dz|_{z_0}$), where z is the axis traversing the interface and z_0 is the position of the interface at which $\rho = (\rho_A + \rho_B)/2$, is related to σ_s as follows:

$$t_I = \sqrt{2\pi}\sigma_s \quad \text{(A3)}$$

We use the Gaussian distribution for the radius of sphere upon averaging so that $\langle f^n(q) \rangle$ is given by

$$\langle f^n(q) \rangle = \frac{\int_0^\infty f^n(q;R) \exp\left[-\frac{(R-\bar{R})^2}{2\sigma_R^2}\right] dR}{\int_0^\infty \exp\left[-\frac{(R-\bar{R})^2}{2\sigma_R^2}\right] dR} \quad \text{(A4)}$$

Here, σ_R is the standard deviation for the distribution of the sphere radius. For the bcc lattice, the lattice factor $Z(q)$ is given by eq A5 with Eulerian angles, θ and ϕ, which define orientation of the bcc unit cell of a given grain with respect to the experimental Cartesian coordinates (X, Y, Z) (see Figure 2 in ref 43):

$$Z(q,\theta,\phi) = \frac{(1-F_k^2)^3}{\left[1 - 2F_k\cos\left(\frac{\sqrt{6}}{4}qd\alpha\right) + F_k^2\right]\left[1 - 2F_k\cos\left(\frac{\sqrt{6}}{4}qd\beta\right) + F_k^2\right]\left[1 - 2F_k\cos\left(\frac{\sqrt{6}}{4}qd\gamma\right) + F_k^2\right]} \quad \text{(A5)}$$

where

$$F_k = \exp\left[-\frac{3}{16} g^2 d^2 q^2 (\alpha^2 + \beta^2 + \gamma^2)\right] \quad \text{(A6)}$$

in which

$$\alpha = \sin\theta\cos\phi + \sin\theta\sin\phi + \cos\theta \quad \text{(A7a)}$$

$$\beta = -\sin\theta\cos\phi - \sin\theta\sin\phi + \cos\theta \quad \text{(A7b)}$$

$$\gamma = -\sin\theta\cos\phi + \sin\theta\sin\phi - \cos\theta \quad \text{(A7c)}$$

In eq A5, d denotes the Bragg spacing which gives rise to the first-order peak and corresponds to the spacing for (110) planes. The paracrystalline distortion factor, g, in eq A6 is defined by $\Delta d/d$, where Δd is the standard deviation of d due to the distortion. For randomly oriented bcc polygrains in the actual samples, the scattering is isotropic. Therefore, $Z(q,\theta,\phi)$ is averaged with respect to θ and ϕ, to obtain isotropic $Z(q)$:

$$Z(q) = \frac{1}{4\pi}\int_0^{2\pi} d\phi \int_0^{\pi} Z(q,\theta,\phi)\sin\theta\, d\theta \quad \text{(A8)}$$

Finally, the volume fraction of spheres packed in the bcc lattice, ϕ_A, is evaluated from the average radius, $\bar{R}$, and the Bragg spacing, d, as given in eq 1.

References and Notes

(1) Helfand, E.; Wasserman, Z. R. In *Developments in Block Copolymers*; Goodman, I., Ed.; Applied Science: New York, 1982; Chapter 4.
(2) Leibler, L. *Macromolecules* **1980**, *13*, 1602.
(3) Fredrickson, G. F.; Helfand, E. *J. Chem. Phys.* **1987**, *87*, 697.
(4) Matsen, M. W.; Schick, M. *Phys. Rev. Lett.* **1994**, *72*, 2660. *Macromolecules* **1994**, *27*, 7157.
(5) Hashimoto, T. In *Thermoplastic Elastomers*; Legge, N. R., Holden, G., Schroeder, H. E., Eds.; Hanser: New York, 1987.
(6) Hashimoto, T.; Tsukahara, Y.; Kawai, H. *J. Polym. Sci., Polym. Lett. Ed.* **1980**, *18*, 585.
(7) Bates, F. S. *Macromolecules* **1984**, *17*, 2607.
(8) Rosadale, J. H.; Bates, F. S. *Macromolecules* **1990**, *23*, 2329.
(9) Bates, F. S.; Rosadale, J. H.; Fredrickson, G. H. *J. Chem. Phys.* **1990**, *92*, 6255.
(10) Bates, F. S.; Fredrickson, G. H. *Annu. Rev. Phys. Chem.* **1990**, *41*, 525.
(11) Han, C. D.; Kim, J. K.; Kim, J. K. *Macromolecules* **1989**, *22*, 383.
(12) Han, C. D.; Baek, D. M.; Kim, J. K. *Macromolecules* **1990**, *23*, 561.
(13) Han, C. D.; Baek, D. M.; Kim, J. K.; Ogawa, T.; Hashimoto, T. *Macromolecules* **1995**, 28, 5043.
(14) Bates, F. S.; Hartney, M. A. *Macromolecules* **1985**, *18*, 2478.
(15) Balsara, N. P.; Perahia, D.; Safinya, C. R.; Tirrell, M.; Lodge, T. P. *Macromolecules* **1992**, *25*, 3896.
(16) Balsara, N. P.; Dai, H. J.; Kesani, P. K.; Garatz, B. A.; Hammouda, B. *Macromolecules* **1994**, *27*, 7406.
(17) Stühn, B. *J. Polym. Sci., Part B: Polym. Phys. Ed.* **1992**, *30*, 1013.
(18) Kasten, H.; Stühn, B. *Macromolecules* **1995**, *28*, 4777.
(19) Hajduk, D. A.; Grunmer, S. M.; Erramilli, S.; Register, R. A.; Fetters, L. J. *Macromolecules* **1996**, *29*, 1473.
(20) Floudas, G.; Hadjichristidis, N.; Stamm, M.; Likthman, A. E.; Semenov, A. N. *J. Chem. Phys.* **1997**, *106*, 3318.
(21) Kim, J. K.; Lee, H. H.; Gu, Q.; Chang, T.; Jeong, Y. H. *Macromolecules* **1998**, *31*, 4045.
(22) Soenen, H.; Liskova, A.; Reynders, K.; Berghmans, H.; Winter, H. H.; Overbergh, N. *Polymer* **1997**, *38*, 5661.
(23) Voronov, V. P.; Buleiko, V. M.; Podneks, V. E.; Hamley, I. W.; Fairclough, J. P. A.; Ryan, A. J.; Mai, S. M.; Kiao, B. X.; Booth, C. *Macromolecules* **1997**, *30*, 6674.
(24) Sakamoto, N.; Hashimoto, T.; Han, C. D.; Kim, D.; Vaidya, N. Y. *Macromolecules* **1997**, *30*, 1621.
(25) Sakamoto, N.; Hashimoto, T.; Han, C. D.; Kim, D.; Vaidya, N. Y. *Macromolecules* **1997**, *30*, 5321.
(26) Adams, J. L.; Graessley, W. W.; Register, R. A. *Macromolecules* **1994**, *27*, 6026.
(27) Harkless, C. R.; Singh, M. A.; Nagler, S. E. *Phys. Rev. Lett.* **1990**, *64*, 2285. Singh, M. A.; Harkless, C. R.; Nagler, S. E.; Shannon, Jr., R. F.; Ghosh, S. S. *Phys. Rev. B* **1993**, *47*, 8425.
(28) Hashimoto, T.; Shibayama, M.; Kawai, H.; Watanabe, H.; Kotaka, T. *Macromolecules* **1983**, *16*, 361.
(29) Sakamoto, N.; Hashimoto, T. *Macromolecules* **1998**, *31*, 8493.
(30) Matsen, M. M.; Bates, F. S. *J. Chem. Phys.* **1997**, *106*, 2436.
(31) Mani, S.; Weiss, R. A.; Hahn, S. F.; Williams, C. E.; Cantino, M. E.; Khairallah, L. H. *Polymer* **1998**, *33*, 2023.
(32) Gergen, W. P. *Kautschuk Gummi* **1984**, *37*, 284.
(33) Kim, J. K.; Jung, D. S.; Kim, J. *Polymer* **1993**, *34*, 4613.
(34) Han, J. H.; Feng, D.; Choi-Feng, C.; Han, C. D. *Polymer* **1995**, *36*, 155.
(35) Park, B. J.; Rah, S. Y.; Park, Y. J.; Lee, K. B. *Rev. Sci. Instrum.* **1995**, *66*, 1722.
(36) Shibayama, M.; Hashimoto, T.; Kawai, H. *Macromolecules* **1983**, *16*, 16.
(37) A broad shoulder marked by a thin arrow resulted from the scattering intensity, $I(q)$, which is proportional to $Z(q)$ times $f(q)$. Here, $Z(q)$ and $f(q)$ are the scattering amplitudes due to the lattice factor (interparticle interference) and to the particle factor (intraparticle interference), respectively, and given in eqs A8 and A2 in the Appendix. From eq A2, $f(q)$ decreases gradually starting from $q = 0$ to $q \sim 0.5$ nm^{-1} and then exhibits a small maximum at $q \sim 0.77$ nm^{-1}.[38] But, the contribution of the lattice scattering at $q \sim 0.45$ nm^{-1} becomes very small. Thus, it is expected to appear a broad shoulder at $q \sim 0.45$ nm^{-1} from these two combining results. Therefore, we attributed the appearance of a shoulder at $q \sim 0.45$ nm^{-1} to the tail of the zeroth-order particle scattering peak, $f(q=0)$, from spheres in LSO. This kind of a broad shoulder was reported previously for an asymmetric block copolymer with spheres in LSO.[24,27,39]
(38) Umeda, H.; Sakurai, S.; Kitagawa, Y.; Suda, Y.; Masamoto, J.; Nomura, S. *Kobunshi Ronbunshu (Japan)* **1997**, *54*, 236.
(39) Schwab, M.; Stühn, B. *Phys. Rev. Lett.* **1996**, *76*, 924.
(40) Doi, M.; Edwards, S. F. *The Theory of Polymer Dynamics*; Clarendon Press: Oxford, 1986.
(41) Fetters, L. J.; Lohse, D. J.; Richter, D.; Witten, T. A.; Zirkel, A. *Macromolecules* **1994**, *27*, 4639.
(42) Hosemann, R.; Bagchi, S. N. In *Direct Analysis of Diffraction by Matter*; North-Holland: Amsterdam, 1962.
(43) Matsuoka, H.; Tanaka, H.; Hashimoto, T.; Ise, N. *Phys. Rev. B* **1987**, *36*, 1754.
(44) Matsuoka, H.; Tanaka, H.; Iizuka, N.; Hashimoto, T.; Ise, N. *Phys. Rev. B* **1990**, *41*, 3854.
(45) Semenov, A. N. *Macromolecules* **1989**, *22*, 2849.
(46) de la Cruz, M. O. *Phys. Rev. Lett.* **1991**, *67*, 85.
(47) Kim, J. K.; Lee, H. H.; Ree, M.; Lee, K. B.; Park, Y. *Macromol. Chem. Phys.* **1998**, *199*, 641.
(48) Adams, J. L.; Quiram, D. J.; Graessley, W. W.; Register R. A.; Marchand, G. R. *Macromolecules* **1996**, *29*, 2929.
(49) Koppi, K. A.; Tirrell, M.; Bates, F. S.; Almdal, K.; Mortensen, K. *J. Rheol.* **1994**, *38*, 999.
(50) Kossuth, M. B.; Morse, D. C.; Bates, F. S. *J. Rheol.* **1999**, *43*, 167.
(51) Palerne, J. F. *Rheol. Acta* **1990**, *29*, 204.
(52) Graebling, D.; Muller, R.; Palerne, J. F. *Macromolecules* **1993**, *26*, 320.

MA9902854